

Schizandrin A can inhibit non-small cell lung cancer cell proliferation by inducing cell cycle arrest, apoptosis and autophagy

LINHAI ZHU¹, YING WANG², WANG LV¹, XIAO WU¹, HONGXU SHENG¹, CHENG HE¹ and JIAN HU¹

¹Department of Thoracic Surgery and ²Operating Room, The First Affiliated Hospital, School of Medicine, Zhejiang University, Hangzhou, Zhejiang 310003, P.R. China

Received June 6, 2021; Accepted September 9, 2021

DOI: 10.3892/ijmm.2021.5047

Abstract. Schizandrin A (SchA) can be extracted from the vine plant *Schisandra chinensis* and has been reported to confer various biologically active properties. However, its potential biological effects on non-small cell lung cancer (NSCLC) remain unknown. Therefore, the present study aims to address this issue. NSCLC and normal lung epithelial cell lines were first treated with SchA. Cell viability and proliferation were measured using CellTiter-Glo Assay and colony formation assays, respectively. PI staining was used to measure cell cycle distribution. Cell cycle-related proteins p53, p21, cyclin D1, CDK4, CDK6, cyclin E1, cyclin E2, CDK2 and DNA damage-related protein SOX4 were detected by western blot analysis. Annexin V-FITC/PI staining, DNA electrophoresis and Hoechst 33342/PI dual staining were used to detect apoptosis. JC-1 and DCFH-DA fluorescent dyes were used to measure the mitochondrial membrane potential and reactive oxygen species concentrations, respectively. Apoptosis-related proteins caspase-3, cleaved caspase-3, poly(ADP-ribose) polymerase (PARP), cleaved PARP, BimEL, BimL, BimS, Bcl2, Bax, caspase-9 and cleaved caspas-9 were measured by western blot analysis. Dansylcadaverine was used to detect the presence of the acidic lysosomal vesicles. The expression levels of the autophagy-related proteins LC3-I/II, p62/SQSTM1 and AMPK α activation were measured using western blot analysis. In addition, the autophagy inhibitor 3-methyladenine was used to inhibit autophagy. SchA treatment was found to reduce NSCLC cell viability whilst inhibiting cell proliferation. Low concentrations of SchA (10-20 μ M) mainly induced G₁/S-phase cell cycle arrest. By contrast, as the concentration of SchA used increases (20-50 μ M), cells underwent apoptosis

and G₂/M-phase cell cycle arrest. As the treatment concentration of SchA increased from 0 to 50 μ M, the expression of p53 and SOX4 protein also concomitantly increased, but the expression of p21 protein was increased by 10 μ M SchA and decreased by higher concentrations (20-50 μ M). In addition, the mRNA and protein expression levels of Bcl-like 11 (Bim) EL, BimL and BimS increased following SchA application. SchA induced the accumulation of acidic vesicles and induced a marked increase in the expression of LC3-II protein, suggesting that SchA activated the autophagy pathway. However, the expression of the p62 protein was found to be increased by SchA, suggesting that p62 was not degraded during the autophagic flux. The 3-methyladenine exerted no notable effects on SchA-induced apoptosis. Taken together, results from the present study suggest that SchA exerted inhibitory effects on NSCLC physiology by inducing cell cycle arrest and apoptosis. In addition, SchA partially induced autophagy, which did not result in any cytoprotective effects.

Introduction

According to the 'World Cancer Report 2020' released by the World Health Organization International Agency for Research on Cancer, lung cancer (1.8 million cases per year) remains to be the leading cause of cancer-associated mortality (1). Non-small cell lung cancer (NSCLC), including lung squamous cell carcinoma, lung adenocarcinoma and large cell carcinoma, is the most common type of lung cancer, accounting for ~85% of all cases (2). Significant progress has been achieved in the development of treatment methods for NSCLC over the past decade. The clinical application of molecularly targeted drugs, including gefitinib, osimertinib, crizotinib and loratinib and immune checkpoint inhibitors, such as nivolumab and pembrolizumab, has significantly prolonged the survival time of patients with advance NSCLC (3,4). However, NSCLC cells can develop resistance to these targeted therapy or immunotherapy, thereby resuming disease progression (5-7). Therefore, drug resistance has become a major obstacle to the survival of patients with NSCLC (5-7). At present the primary strategy to address drug resistance is by either combining multiple antitumor agents or by identifying novel therapeutic agents specifically targeting the mechanism underlying drug

Correspondence to: Professor Jian Hu, Department of Thoracic Surgery, The First Affiliated Hospital, School of Medicine, Zhejiang University, 79 Qingchun Road, Hangzhou, Zhejiang 310003, P.R. China
E-mail: dr_hujian@zju.edu.cn

Key words: non-small cell lung cancer, schizandrin A, cell cycle arrest, apoptosis, autophagy

resistance (8-10). However, adverse side effects following multi-drug therapy limit its clinical application (10,11). Therefore, investigating novel effective therapeutic strategies is essential for overcoming drug resistance and prolong the survival of patients with lung cancer.

By gaining an in-depth understanding of the cancer pathological mechanism, targeted therapeutic drugs can be designed and developed based on the specific physiological characteristics of the cancer (12). However, screening existing compounds or naturally occurring medicinal compounds for potential therapeutic effects on cancer remains to be an indispensable part of cancer treatment research. Vinblastine (13), platinum compounds (14) and paclitaxel (15) are all examples of anti-cancer agents that can be found naturally. In addition, monomer compounds purified from natural products also form part of the drug screening libraries (16-18). Their biological activities on various processes, including inflammation, infection and cancer development, have been extensively investigated (19).

Schizandrin A (SchA), also known as deoxyschizandrin, is one of the most biologically active lignans isolated from the fruit of the medicinal vine plant *Schisandra chinensis* (20). Wang *et al* previously revealed that male Sprague-Dawley rats fed with an extract of *Schisandra chinensis* (50 mg/kg) retained detectable levels of SchA in the plasma 6 h after feeding (21). Since SchA has symmetrical methoxy and methyl groups, the loss of these groups forms part of the catabolic mechanism of SchA when it is broken down (22). Based on the results from another pharmacokinetic study into Schizandrol A, Liu *et al* (23) found that hydroxylation and demethylation may also occur when SchA is broken down.

Previous pharmacological studies have reported that SchA has a variety of biologically active properties. Anti-inflammatory (24-27) and antiviral effects (28,29) of SchA and its analogs were initially found. However, it was subsequently found that SchA also confers antitumor (30,31), anti-allergy (32) and anti-fibrosis (33) effects whilst enhancing immunity (34). Over the past decade, studies investigating the potential antitumor effects of SchA have been gradually increasing. It was previously reported that SchA can inhibit cell proliferation, induce cell apoptosis, inhibit cell invasion and tumor metastasis in breast cancer, ovarian cancer, choriocarcinoma, thyroid cancer and colorectal cancer (31,35-42), in addition to enhancing drug efficacy in NSCLC and colon carcinoma (43,44) or overcome drug resistance in breast cancer and esophageal carcinoma (30,45,46). In particular, Xian *et al* revealed that SchA combined with gefitinib could inhibit proliferation whilst promoting apoptosis in gefitinib-resistant NSCLC cells (43). However, the underlying mechanistic effects of SchA on NSCLC remain poorly understood. Therefore, the potential biological effects of SchA on NSCLC was investigated in the present study.

Materials and methods

Cell culture and treatment. The human NSCLC cell lines A549, H1299 and H1975 and the normal human lung epithelial cell lines BEAS-2B were purchased from The Cell Bank of Type Culture Collection of The Chinese Academy of Sciences. RPMI-1640 medium and PBS were purchased from Corning,

Inc. and FBS was purchased from PAN-Biotech GmbH (cat. no. P30-3302). All cell lines were cultured in RPMI-1640 medium supplemented with 10% FBS at 37°C in a humidified atmosphere with 5% CO₂. SchA, with a purity of >98%, was purchased from Chengdu Must Bio-Technology Co., Ltd. (cat. no. 19092908). SchA was dissolved DMSO at a concentration of 50 mM for subsequent experiments.

Cell viability assay. The A549, H1299, H1975 and BEAS-2B cell lines were seeded into a 96-well plate at a density of 3,000 cells per well and incubated at 37°C overnight. For concentration dependence experiments, different concentrations of SchA (0, 25, 50, 75 and 100 μM) or an equal volume of DMSO were added to the cell culture medium to treat the cells for 24 h at 37°C. For time dependence experiments, the cells were treated with 50 μM SchA for 0, 12, 24, 36 and 48 h at 37°C. A Cell Titer-Glo Luminescence Viability Assay kit (cat. no. G7571; Promega Corporation) was used to detect cell viability according to the manufacturer's protocol. Each concentration and time dependence assay was repeated three times. The IC₅₀ and its 95% confidence interval of SchA was evaluated using best-fit dose-response inhibition curves with GraphPad Prism v7.0 Software (GraphPad Software, Inc.).

Cell colony formation assay. The effect of SchA on cell colony formation was evaluated using colony formation assays. Single-cell suspensions of A549 and H1975 were seeded into a six-well plates at a density of 800 cells/well. After the cells adhered, SchA at concentrations of 0, 25 and 50 μM was added into the culture medium. The cells were placed in an incubator and cultured for 10-14 days at 37°C until a single cell clone contained ~50 cells. The colonies were then fixed with 4% paraformaldehyde for 1 h at room temperature and stained with 0.2% crystal violet for 20 min (Sigma-Aldrich; Merck KGaA) at room temperature. The number of colonies visible to the naked eye (Each colony contains >50 cells; x1 magnification) were counted using ImageJ v2 software (ImageJ; National Institutes of Health).

Cell cycle analysis using flow cytometry. The cells were trypsinized with trypsin and centrifuged at 300 x g for 3 min at room temperature, before being re-suspended in 1 ml pre-chilled 70% ethanol. After fixation overnight at -20°C, the cells were re-suspended and stained with 500 μl PI/RNase staining buffer (cat. no. 550825; BD Biosciences) at a density of 1x10⁶ cells/ml at room temperature for 30 min. The cells were then detected using a CytoFLEX analysis flow cytometer (Beckman Coulter, Inc.) and the FL2-A: B610-ECD channel. The results were analyzed using the FlowJo v10 software (FlowJo LLC).

Cell apoptosis analysis using flow cytometry. After the A549 and H1975 cells were treated with SchA (0, 25 and 50 μM) for 24 h at 37°C, the cells were trypsinized without EDTA (cat. no. CR27250; Guangzhou Ruisen Biotechnology Co., Ltd.). After washing twice with pre-chilled PBS, the cells were re-suspended in 1X buffer provided in the FITC Annexin V Apoptosis Detection kit (cat. no. 556547; BD Biosciences) to 1x10⁶ cells/ml. Next, 100 μl cell suspension was added to a flow cytometry tube and 5 μl Annexin V-FITC and 5 μl PI staining solution (cat. no. 556547; BD Biosciences) was added.

The samples were incubated at room temperature for 15 min in the dark, before 400 μ l 1X buffer provided in the kit was added. A CytoFLEX analysis flow cytometer (Beckman Coulter, Inc.) and the FL1-A: B525-FITC and FL4-A: Y585-PE channels were used to measure cell apoptosis, where the results were analyzed using the FlowJo v10 software (FlowJo LLC).

The A549 and H1975 cells were also treated with 5 mM 3-MA for 4 h at 37°C and then treated with 50 μ M SchA for 24 h at 37°C. The apoptosis of the cells was measured by the FITC Annexin V Apoptosis Detection kit (cat. no. 556547; BD Biosciences) and a CytoFLEX analysis flow cytometer (Beckman Coulter, Inc.). The results of apoptosis were also analyzed using the FlowJo v10 software (FlowJo LLC).

DNA electrophoresis. A DNeasy Blood & Tissue kit (cat. no. 69504; Qiagen GmbH) was used to extract DNA from the cells based on the manufacturer's protocols. The DNA sample was mixed with 10X loading buffer (cat. no. 317051; Vazyme Biotech Co., Ltd.) at a ratio of 9:1 before being separated in 1% agarose gels with the 0.01% Ultra GelRed nucleic acid stain (cat. no. GR501-01; Vazyme Biotech Co., Ltd.). A 200-bp DNA Ladder (cat. no. 3423A; Takara Bio, Inc.) was used to calculate the size of the DNA molecules. The FluorChem FC3 System (ProteinSimple) was used for gel imaging and the AlphaView v1.0 software (ProteinSimple) was used to analyze the density of the DNA bands.

Hoechst 33342 and PI staining. The single-cell suspensions of A549 and H1975 were seeded into six-well plates at a density of 2×10^5 cells/well. After the cells were treated with SchA (0, 25 and 50 μ M) for 24 h at 37°C, the cells were washed twice with PBS and incubated with Hoechst 33342 (1 μ g/ml; cat. no. C1029; Beyotime Institute of Biotechnology) for 15 min at room temperature, followed by incubation with PI (5 μ g/ml) for another 15 min at room temperature. Subsequently, the cells were washed three times with PBS and the blue and red fluorescence emitted by the cells was observed. Images were captured using a fluorescence microscope (Leica Microsystems GmbH) at x200 magnification. Image-Pro Plus v6.0 software (Media Cybernetics, Inc.) was used to merge the monochromatic fluorescence images.

Detection of mitochondrial membrane potential (MMP). A MMP Detection kit (MitoScreen; cat. no. 551302; BD Biosciences) was used to measure the level of damage to the MMP in the cell. The JC-1 dye was diluted into a JC-1 working solution according to the manufacturer's protocol. The cells were re-suspended with the JC-1 working solution at a density of 1×10^6 cells/ml and incubated at 37°C for 15 min. After staining, the cells were centrifuged at 240 x g for 3 min and washed twice with 1X buffer provided in the kit. The cells were re-suspended in 500 μ l 1X buffer provided in the kit and detected using a CytoFLEX analysis flow cytometer (Beckman Coulter, Inc.), with the FL1-A: B525-FITC and FL4-A: Y585-PE channels. Red JC-1 dye fluorescence represents live cells with intact MMP whereas green JC-1 monomer fluorescence represents apoptotic or dead cells with impaired MMP. The ratio of red (JC-1 aggregates) to green (JC-1 monomers) fluorescence intensity was used to assess MMP using the FlowJo v10 software (BD Biosciences).

Detection of reactive oxygen species (ROS). The single-cell suspensions of A549 and H1975 were seeded into a six-well plates at a density of 2×10^5 cells/well. The cells were treated with SchA (0, 25 and 50 μ M) for 24 h at 37°C, then ROS probe DCFH-DA (cat. no. 287810; Sigma-Aldrich; Merck KGaA) was added to the cell culture medium at 1:1,000 before the cells were incubated at 37°C for 20 min and washed twice with PBS. Intracellular ROS levels were detected using a fluorescence microscope at x200 magnification (Leica Microsystems GmbH).

After the cells were treated with SchA (0, 25 and 50 μ M) for 24 h at 37°C, the cells were trypsinized to form a single cell suspension with trypsin and re-suspended. The cells were re-suspended in medium containing 0.1% DCFH-DA at a density of 1×10^6 cells/ml and incubated at 37°C for 20 min. They were then washed twice with PBS and re-suspended with 500 μ l PBS after centrifugation at 240 x g for 3 min at 37°C. The FL1-A: B525-FITC channel in a CytoFLEX analysis flow cytometer (Beckman Coulter, Inc.) was used to detect the level of intracellular ROS. The flow cytometry data was analyzed using the FlowJo v10 software (FlowJo LLC).

Staining with Dansylcadaverine (MDC) and Hoechst 33342. MDC was purchased from Sigma-Aldrich (cat. no. 10121-91-2; Sigma-Aldrich; Merck KGaA). The single-cell suspensions of A549 and H1975 were seeded into a six-well plates at a density of 2×10^5 cells/well. After treatment with SchA (0, 25, 50 μ M) for 24 h at 37°C, the cells were washed twice with PBS and incubated with MDC (final concentration, 0.05 mM) and Hoechst 33342 (final concentration, 1 μ g/ml) for 15 min at room temperature in the dark. After washing the cells three times with PBS, the green and blue fluorescence emitted by the cells, was observed. Images were captured using a fluorescence microscope at x200 magnification (Leica Microsystems GmbH). Image-Pro Plus v6.0 software (Media Cybernetics, Inc.) was used to merge the monochrome fluorescent images. Autophagy inhibitor 3-methyladenine (3-MA) was purchased from Sigma-Aldrich (cat. no. M9281; Sigma-Aldrich; Merck KGaA).

Measurement of ATP levels. The ATP levels were assessed by ATP Detection Assay kit (cat. no. 700410, Cayman Chemical Company) according to the manufacturer's protocols. The single-cell suspensions of A549 and H1975 were seeded into a six-well plates at a density of 2×10^5 cells/well. After the cells were treated with SchA (0, 25 and 50 μ M) for 24 h at 37°C, the cell culture medium was first discarded and the cells were washed with pre-chilled PBS before 1 ml 1X sample buffer was added to each well (6-well plate) to lyse the cells. D-luciferin and luciferase were added to the ATP detection buffer to prepare the reaction mixture. The detection holes on the black 96-well plates and three duplicate wells for each sample were organized. A total of 100 μ l freshly prepared reaction mixture and 10 μ l cell lysate were added to each well, mixed and incubated for 15 min in the dark at room temperature. A multifunctional microplate reader was used to measure the fluorescence value in each well. GraphPad Prism v7.0 software (GraphPad Software, Inc.) was used to generate a histogram to show the fluorescence values.

Western blot analysis. The cells were lysed using the RIPA Lysis Buffer (cat. no. P0013B; Beyotime Institute of Biotechnology)

containing the Protease Inhibitor Cocktail (cat. no. 05892791001; Roche Diagnostics GmbH) and Phosphatase Inhibitor Cocktail (cat. no. 524629; EMD Millipore). The BCA Protein Assay kit (cat. no. PC0020; Beijing Solarbio Science & Technology Co., Ltd.) was used to determine protein concentration. Loading buffer (5X) was then added to the protein lysate at a ratio of 1:4. A total of 30 μg protein sample per line was separated using 12% SDS-PAGE and then transferred onto PVDF membranes (EMD Millipore). The membranes were blocked with 5% BSA (cat. no. 97061-422; VWR International) in TBS-0.1% Tween-20 (TBST) before being incubated with primary antibodies on a shaker overnight at 4°C. The p53 (cat. no. 2527), p21 (cat. no. 2947), cyclin D1 (cat. no. 2922), CDK4 (cat. no. 12790), CDK6 (cat. no. 13331), cyclin E1 (cat. no. 20808), cyclin E2 (cat. no. 4132), CDK2 (cat. no. 2546), caspase-3 (cat. no. 14220), poly (ADP-ribose) polymerase (PARP; cat. no. 9542), Bcl2-like 11 (Bim; cat. no. 2933), Bcl2 (cat. no. 4223), Bax (cat. no. 5023), caspase-9 (cat. no. 9502), LC3 (cat. no. 4108), p62 (cat. no. 8025), phosphorylated (p-) AMPK α -T172 (cat. no. 2535) and AMPK α (cat. no. 5831) antibodies were purchased from Cell Signaling Technology, Inc. The primary antibodies against SOX4 (cat. no. DF2610; Affinity Biosciences) and β -actin (cat. no. A1978; Sigma-Aldrich; Merck KGaA) were also used. All primary antibodies were diluted in primary antibody dilution buffer (cat. no. P0256; Beyotime Institute of Biotechnology) at a ratio of 1:1,000. The membrane were washed three times with TBST and then incubated with HRP-conjugated anti-rabbit (cat. no. 7074; Cell Signaling Technology, Inc.) or anti-mouse (cat. no. 7076; Cell Signaling Technology, Inc.) secondary antibodies at room temperature for 1 h. After washing the membrane three times with TBST, an ECL kit chemiluminescent substrate (cat. no. BL523B; Biosharp Life Sciences) was used to visualize the protein bands.

Total RNA extraction and PCR. Total RNA was extracted using a RNA Quick Purification kit (cat. no. ES-RN001; Shanghai YiShan Biotechnology Co., Ltd.) and reverse transcribed into single-strand cDNA using a HiScript II Q RT SuperMix kit (cat. no. R223; Vazyme Biotechnology Co., Ltd.) at 50°C for 15 min, followed by 85°C for 5 sec. Quantitative PCR (qPCR) was performed using the PowerUp™ SYBR™-Green Master Mix (cat. no. A25742; Thermo Fisher Co., Ltd.) and an Applied Biosystems 7500 Fast Real-Time PCR System (Thermo Fisher Scientific, Inc.). The thermocycling conditions of qPCR were set as follows: 95°C for 1 min, followed by 95°C for 10 sec, 60°C for 20 sec and 72°C for 30 sec for 40 cycles. Relative expression levels were calculated by the $2^{-\Delta\Delta C_q}$ method normalized to the internal reference gene β -actin (47).

Reverse transcription (RT)-semiquantitative PCR (RT-PCR) was conducted using 2X Taq Master mix (cat. no. P112; Vazyme Biotech Co., Ltd.) and a Bio-Rad T100 thermal cycler (Bio-Rad Laboratories, Inc.). The thermocycling conditions of RT-PCR were set as follows: 95°C for 3 min, followed by 95°C for 15 sec, 60°C for 15 sec and 72°C for 60 sec for 25 cycles. The primer sequences were as follows: Bim forward, 5'-TAAGTTCTGAGTGTGACCGAGA-3' and reverse, 5'-GCTCTGTCTGTA GGGAGGTAGG-3'; Bim (BimEL, BimL and BimS), which contained exons 2 and 5 (48), forward, 5'-ATGGCAAAGC AACCTTCTGA-3' and reverse, 5'-TCAATGCATTCTCCACA CCA-3' and β -actin forward, 5'-CATGTACGTTGCTATCCA GGC-3' and reverse, 5'-CTCCTTAATGTCACGCACGAT-3'.

A total of 10 μg DNA per lane was separated using 1% agarose gel and stained with 0.01% Ultra GelRed nucleic acid stain (cat. no. GR501-01; Vazyme Biotech Co., Ltd.).

Statistical analysis. All experiments were repeated 3 times for each assay and the results were presented as the mean \pm SD. One-way ANOVA was used to evaluate the quantitative data for statistical significance, then Dunnett's test was used for multiple comparisons. $P < 0.05$ was considered to indicate a statistically significant difference.

Results

SchA reduces cell viability and inhibits the proliferation of NSCLC cells. The 2D and 3D structures of SchA (PubChem compound ID, 43595; $\text{C}_{24}\text{H}_{32}\text{O}_6$; molecular weight, 416.5 g/mol) are shown in Fig. 1A and B. SchA belongs to the dibenzocyclooctadiene family of lignans (49). Its main feature is that the biaryl units are connected via aliphatic chains to form an eight-membered ring carbon skeleton (50).

The CellTiter-Glo assay was used to measure the viability of cells treated with different concentrations of SchA (0, 25, 50, 75 and 100 μM) for 24 h. The results showed that SchA exerted inhibitory effects on the viability of A549, H1975, H1299 and BEAS-2B cells in a concentration-dependent manner (Fig. 1C). The IC_{50} and its 95% confidence interval (CI) were used to evaluate the ability of SchA to inhibit cell viability. The IC_{50} and 95% CI in the A549, H1299, H1975 and BEAS-2B cell lines were 61.09 (44.47-177.0), 101.5 (65.45-529.2), 39.99 (33.48-59.28) and 49.45 (44.84-57.16) μM , respectively. The A549 and H1975 cell lines appeared to be more sensitive to SchA, whilst the H1299 cell line was more resistant. As the treatment time with 50 μM SchA was prolonged (0, 12, 24, 36 and 48 h), the viability of the A549 and H1975 cell lines was also markedly reduced (Fig. 1D). SchA (50 μM) exerted a potent inhibitory effect on the viability of A549 and H1975 cells 24 h after treatment (Fig. 1C and D).

Colony formation assay was used to detect the effect of SchA on cell proliferation and colony formation. The results showed that SchA could significantly inhibit the colony formation abilities of A549 and H1975 cells, where this inhibitory effect was concentration-dependent (Fig. 1E and F).

SchA triggers cell cycle arrest in A549 and H1975 cells. The biological process that is most closely associated with cell proliferation is cell mitosis. Therefore, to investigate the effect of SchA on mitosis, the cell cycle was evaluated using flow cytometry after PI staining. After treatment of A549 and H1975 cells with increasing concentrations of SchA (0, 10, 20, 30 and 50 μM) for 24 h, cell cycle progression was assessed. As shown in Fig. 2A and B, after the cells were treated with lower concentrations of SchA (10-20 μM), the percentage of cells in the G_0/G_1 phase was significantly increased. However, after the cells were treated with higher concentrations of SchA (20-50 μM), the percentage of cells in the G_0/G_1 phase was gradually decreased (Fig. 2A and B). Although the percentage of cells in S phase and G_2/M phase gradually increased, no statistical significance could be found. In addition, as the concentration of SchA increased, the proportion of cells in the sub- G_1 phase was also significantly increased. This suggest that lower concentrations

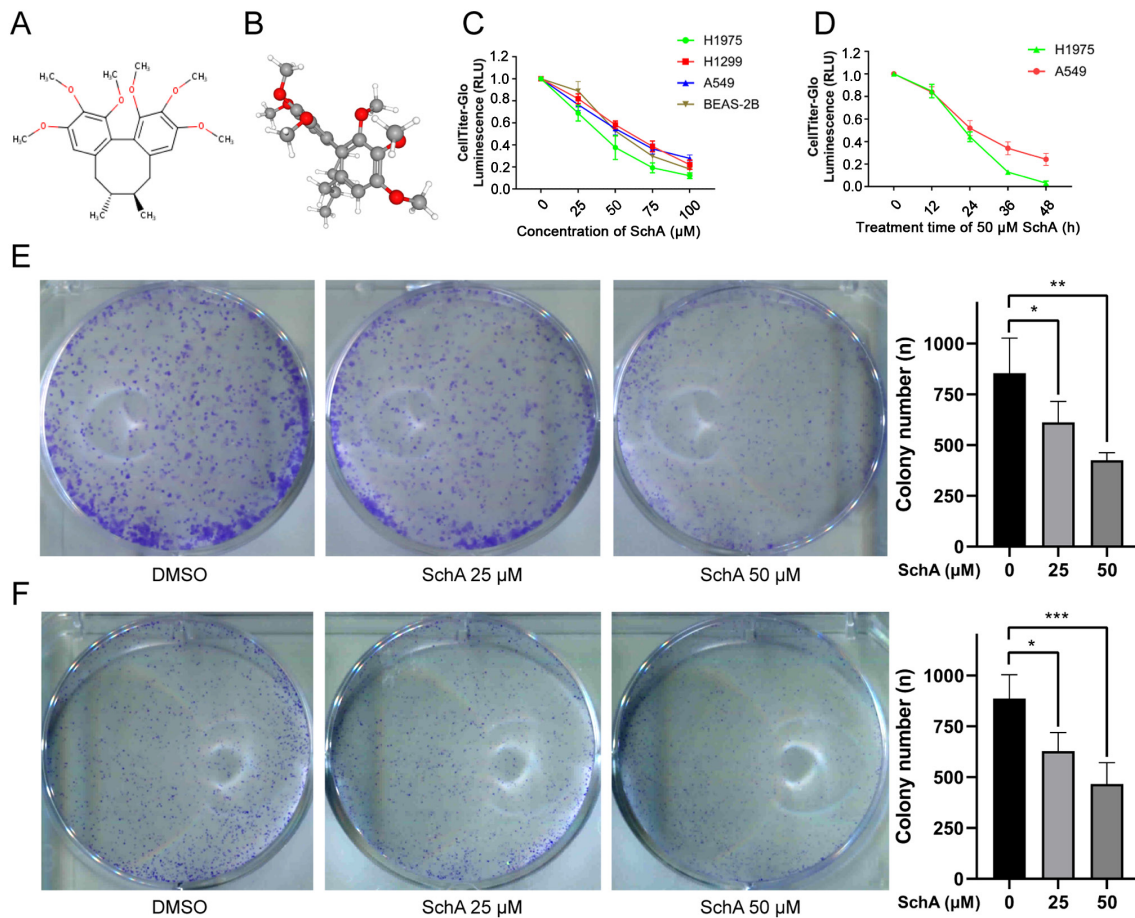


Figure 1. SchA reduces cell viability and inhibits cell proliferation in A549 and H1975 cells. (A) 2D and (B) 3D molecular structure of SchA. (C) SchA (0, 25, 50, 75 and 100 μM) reduced the viability of H1975, H1299, A549 and BEAS-2B cells in a concentration-dependent manner. (D) SchA (50 μM) reduced the viability of H1975 and A549 cells in a time-dependent manner. SchA inhibited colony formation by (E) A549 and (F) H1975 cells, which were observed at x1 magnification. * $P < 0.05$, ** $P < 0.01$ and *** $P < 0.001$; SchA, Schizandrin A; RLU, relative light unit.

of SchA (10–20 μM) can induce G_1/S -phase arrest, whilst higher concentrations of SchA (20–50 μM) can induce apoptosis.

Western blot analysis was subsequently used to measure changes in the expression levels of cell cycle-related proteins. As the concentration of SchA was increased (0, 10, 20, 30 and 50 μM), the protein expression levels of p53, cyclin E2, CDK2 and SOX4 were increased, whilst the protein expression levels of cyclin D1, CDK4, CDK6 and cyclin E1 were decreased (Fig. 2C and D). The protein expression levels of p21 were increased initially, peaking at 10 μM SchA before decreasing again at higher concentrations (Fig. 2C). After the cells were treated with 50 μM SchA for increasing periods time (0, 3, 6, 12 and 24 h), the protein expression levels of p53, cyclin E2, CDK2 and SOX4 were increased, whereas the protein expression levels of p21, cyclin D1, CDK4, CDK6 and cyclin E1 were decreased (Fig. 2D).

SchA induces apoptosis in A549 and H1975 cells. Sub- G_1 cells are hypodiploid cells with an incomplete genome (51). SchA was previously found to increase the percentage of sub- G_1 cells whilst also increasing the expression of the DNA damage-related proteins p53 and SOX4 (52). This suggests that DNA damage and apoptosis occurred in the cells following treatment with SchA. In the present study, the percentage of apoptotic cells was detected using flow cytometry and

Annexin V-FITC/PI double-staining. The results indicated that the number of early and late apoptotic cells was significantly increased with increasing SchA concentrations (Fig. 3A and B). In addition, DNA electrophoresis was used to detect the effect of SchA on DNA integrity. It was found that SchA treatment caused DNA to break into a characteristic ladder-like pattern (Fig. 3C and D). To investigate the apoptosis-related morphological changes, the SchA-treated cells were stained with Hoechst 33342 and PI before being observed using fluorescence microscopy. The results showed that the cells treated with SchA were shrunken, with evidence of fragmentation and emitted irregular dense masses of blue fluorescence (Fig. 3E and F). In addition, PI red fluorescence was also increased by SchA treatment (Fig. 3E and F).

To verify the effects of SchA on apoptosis on the molecular level, western blot analysis was performed to measure changes in the protein expression levels of apoptosis-related proteins in cells treated with SchA. Following SchA treatment, caspase-3 and PARP in A549 and H1975 cells were cleaved, such that the expression levels of cleaved caspase-3 and cleaved PARP were markedly increased (Fig. 3G and H). These findings suggest that SchA induced apoptosis in A549 and H1975 cells.

SchA induces the loss of MMP in the NSCLC cell lines. Mitochondrial damage is one of the key features of apoptotic

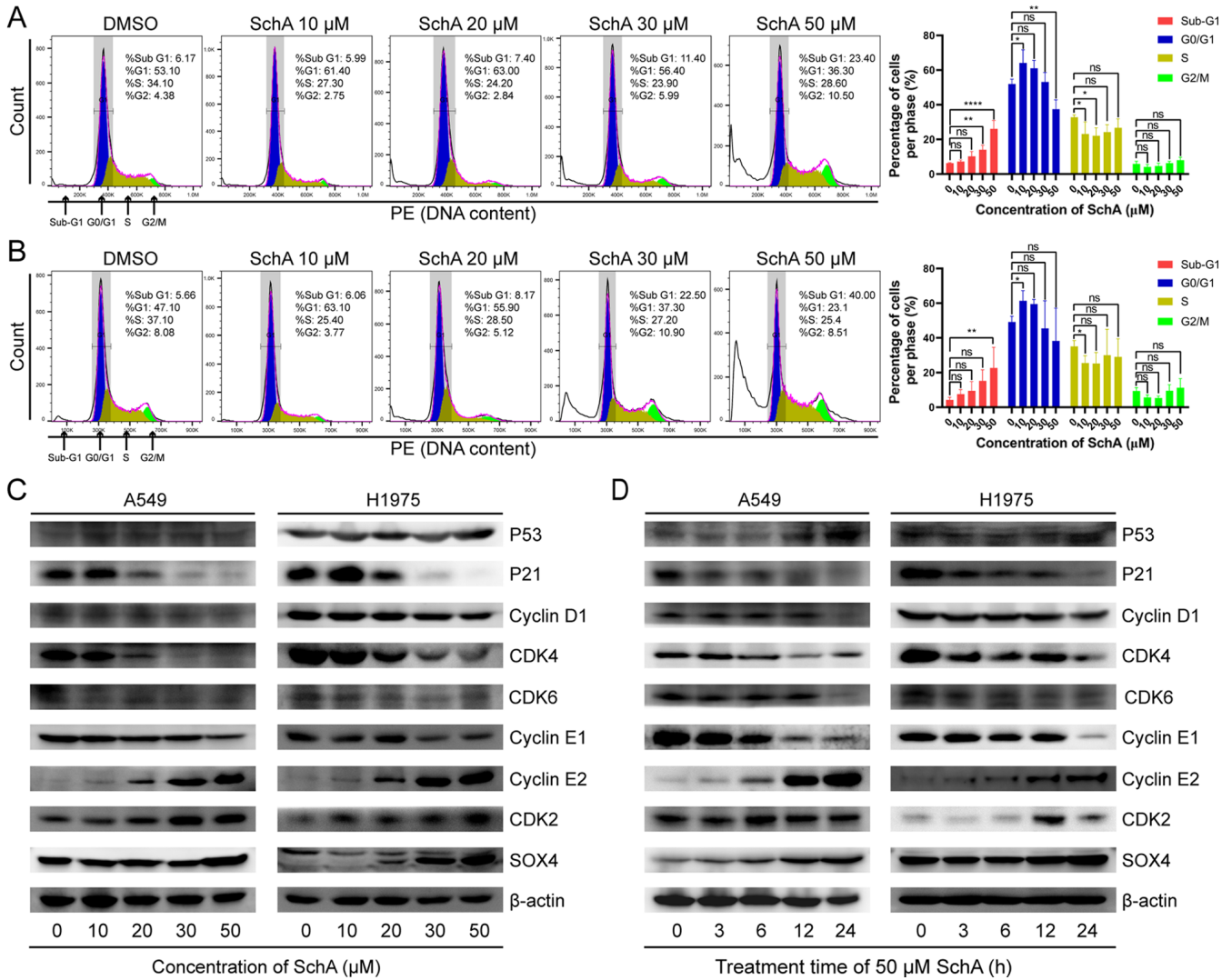


Figure 2. SchA induces cell cycle arrest in A549 and H1975 cells. The effect of SchA on the cell cycle progression of (A) A549 and (B) H1975 cells. The effect of SchA on the protein expression levels of cell cycle regulation proteins in (C) A549 and (D) H1975 cells. * $P < 0.05$, ** $P < 0.01$ and *** $P < 0.0001$. SchA, Schizandrin A; ns, not significant.

cells, where the loss of MMP is an essential manifestation of mitochondrial damage (53). To investigate the effect of SchA on mitochondrial physiology, JC-1 staining was used to detect the integrity of the MMP in A549 and H1975 cells after treatment with SchA. The red JC-1 aggregates represent intact MMP, whilst green JC-1 monomers represents damaged MMP. As the concentration of SchA increased (0, 25 and 50 μ M), the number of cells emitting red fluorescence was decreased, whilst the number of cells emitting green fluorescence was increased (Fig. 4A and B). As a result, there was a significant decrease in the ratio of red (JC-1 aggregates)/green (JC-1 monomers) fluorescence (Fig. 4A and B), suggesting that SchA induced MMP damage in A549 and H1975 cells.

SchA induces changes in the level and distribution of intracellular ROS. Mitochondrial damage leads to impaired oxidative phosphorylation and electron transport chain, which results in excessive ROS production and release from mitochondria (54). Excessive and abnormally distributed ROS can also affect mitochondrial function and reduce cell viability (54). To detect whether the ROS level was affected by SchA, DCFH-DA probes

were used to evaluate intracellular ROS levels in the A549 and H1975 cells. The results of DCFH-DA staining were first detected using flow cytometry (Fig. 4C and D). As the concentration of SchA was increased, the number of cells emitting green fluorescence was also markedly and gradually increased, with the green fluorescence intensity strengthening progressively.

The results of DCFH-DA probe staining were also observed using fluorescence microscopy. As shown in Fig. 4E and F, after SchA treatment DCFH-DA green fluorescence in A549 and H1975 cells increased in intensity, which was widely distributed in the cytoplasm. These findings indicate that SchA increased the levels of intracellular ROS and disrupted the distribution of ROS in A549 and H1975 cells.

SchA induces changes in the expression of mitochondrial apoptosis pathway-related proteins. To verify if SchA induces cell apoptosis by activating the mitochondrial pathway, western blot analysis was used to detect the expression levels of mitochondrial apoptosis pathway-related proteins. As shown in Fig. 4G and H, after SchA treatment the expression levels of pro-apoptotic mitochondrial proteins, BimEL, BimL, BimS

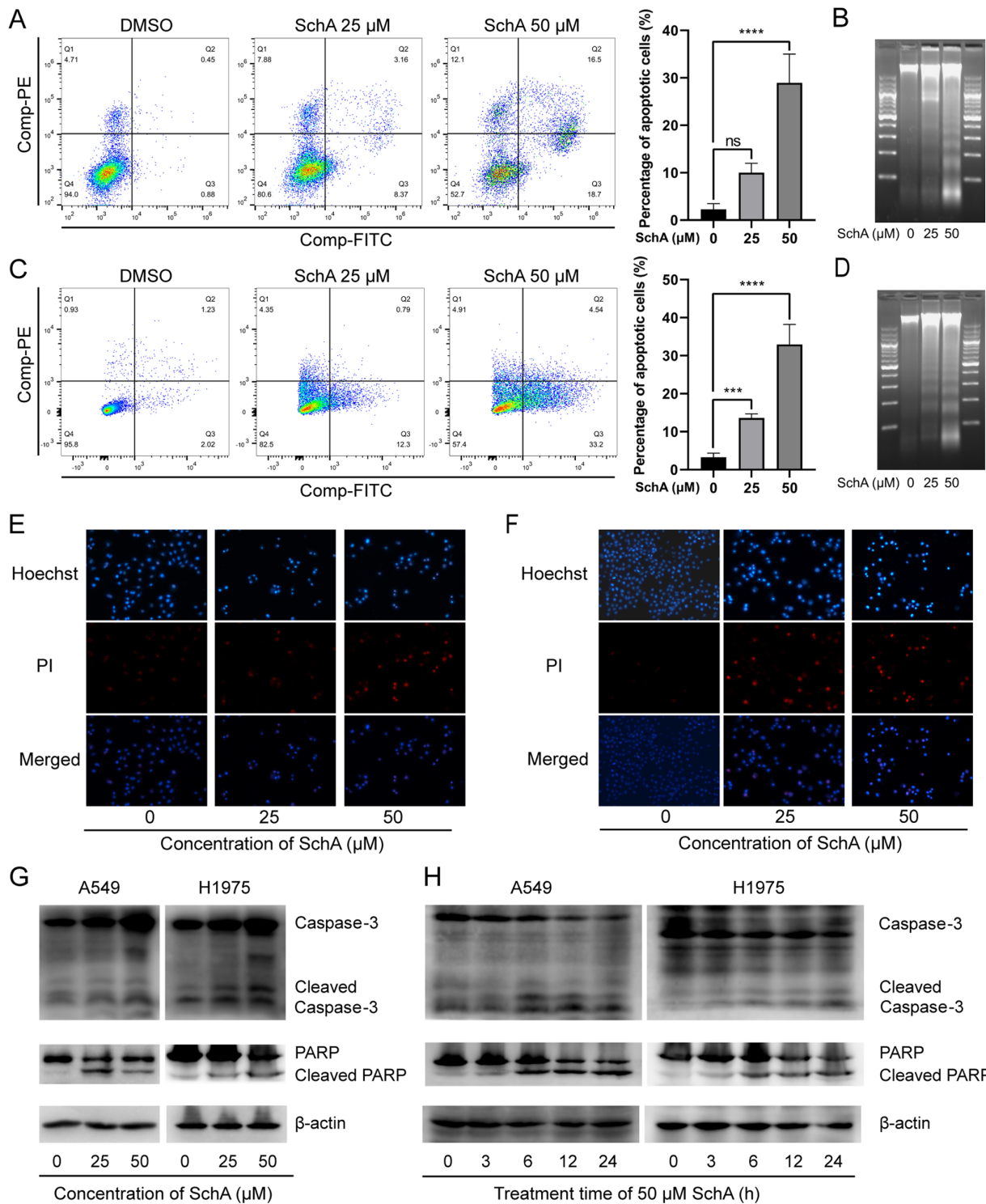


Figure 3. SchA induces apoptosis in A549 and H1975 cells. (A) Flow cytometry following FITC-Annexin V and PI double staining showed that SchA induced apoptosis in A549 cells. (B) DNA electrophoresis showed that SchA caused DNA fragmentation in A549 cells. (C) Flow cytometry following FITC-Annexin V and PI double staining showed that SchA induced apoptosis in H1975 cells. (D) DNA electrophoresis showed that SchA caused DNA fragmentation in H1975 cells. Hoechst 33342 and PI double staining at $\times 200$ magnification showed that SchA caused (E) A549 and (F) H1975 cells emit irregular concentrated blue fluorescence whilst increasing PI absorption. (G) Increasing concentrations of SchA were added to cells and the protein expression levels of apoptotic proteins in the A549 and H1975 cells were analyzed. (H) The time dependency effect of 50 μ M SchA on the protein expression levels of apoptotic proteins in A549 and H1975 cells was analyzed. *** $P < 0.001$ and **** $P < 0.0001$. SchA, Schizandrin A; PARP, poly (ADP-ribose) polymerase; ns, not significant.

and Bax in A549 and H1975 cells were markedly increased. By contrast, the expression level of the anti-apoptotic protein Bcl-2 was decreased. In addition, the expression level of mitochondrial apoptosis biomarker, cleaved-caspase 9 (55), was markedly increased.

Bim is involved in sensing cellular stress and initiates the mitochondrial apoptosis pathway (56). Bim gene transcription typically increases after the cellular stress response and is expressed in the form of various alternative splice variants, including BimEL, BimL and BimS (48,57).

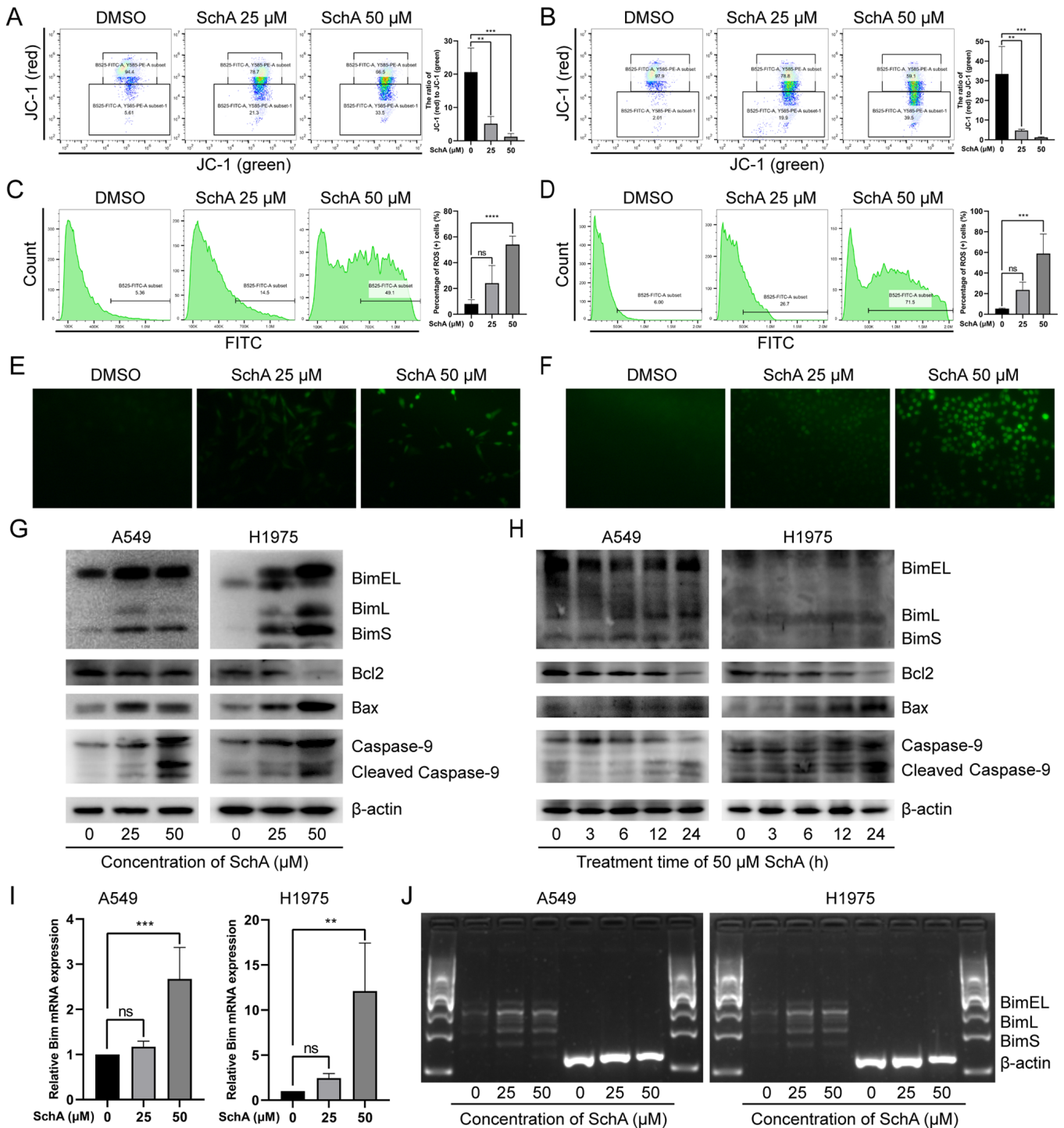


Figure 4. SchA activates the mitochondrial apoptosis pathway in A549 and H1975 cells. JC-1 staining showed that SchA treatment damaged the mitochondrial membrane potential in (A) A549 and (B) H1975 cells. The results of DCFH-DA staining observed using flow cytometry showed that SchA significantly increased the level of ROS in (C) A549 and (D) H1975 cells. The results of DCFH-DA staining observed using a fluorescence microscopy at $\times 200$ magnification showed that SchA enhanced green fluorescence and hence ROS levels in (E) A549 and (F) H1975 cells. (G) The dose dependency and (H) time dependency effects of SchA on the expression levels of proteins associated with the mitochondrial apoptosis pathway were measured in A549 and H1975 cells using western blotting. (I) The effect of SchA on the mRNA expression levels of Bim in A549 and H1975 cells. (J) The effect of SchA on the mRNA expression levels of BimEL, BimL and BimS in A549 and H1975 cells. ** $P < 0.01$ and *** $P < 0.001$; **** $P < 0.0001$. SchA, Schizandrin A; ns, not significant; Bim, Bcl2-like 11.

Subsequently, it was found that the protein expression levels of BimEL, BimL and BimS in the cells were increased after SchA treatment. This may be due to reduced degradation or increased expression of the Bim protein. To detect the effect of SchA on the mRNA expression level of the *Bim* gene, RT-qPCR was used to detect the mRNA expression

levels of Bim. As shown in Fig. 4I, SchA increased the mRNA expression levels of total Bim in A549 and H1975 cells. In addition, the expression of the mRNA levels of BimEL, BimL and BimS in the A549 and H1975 cells were also measured through RT-PCR. It was found that the mRNA expression levels of BimEL, BimL and BimS were

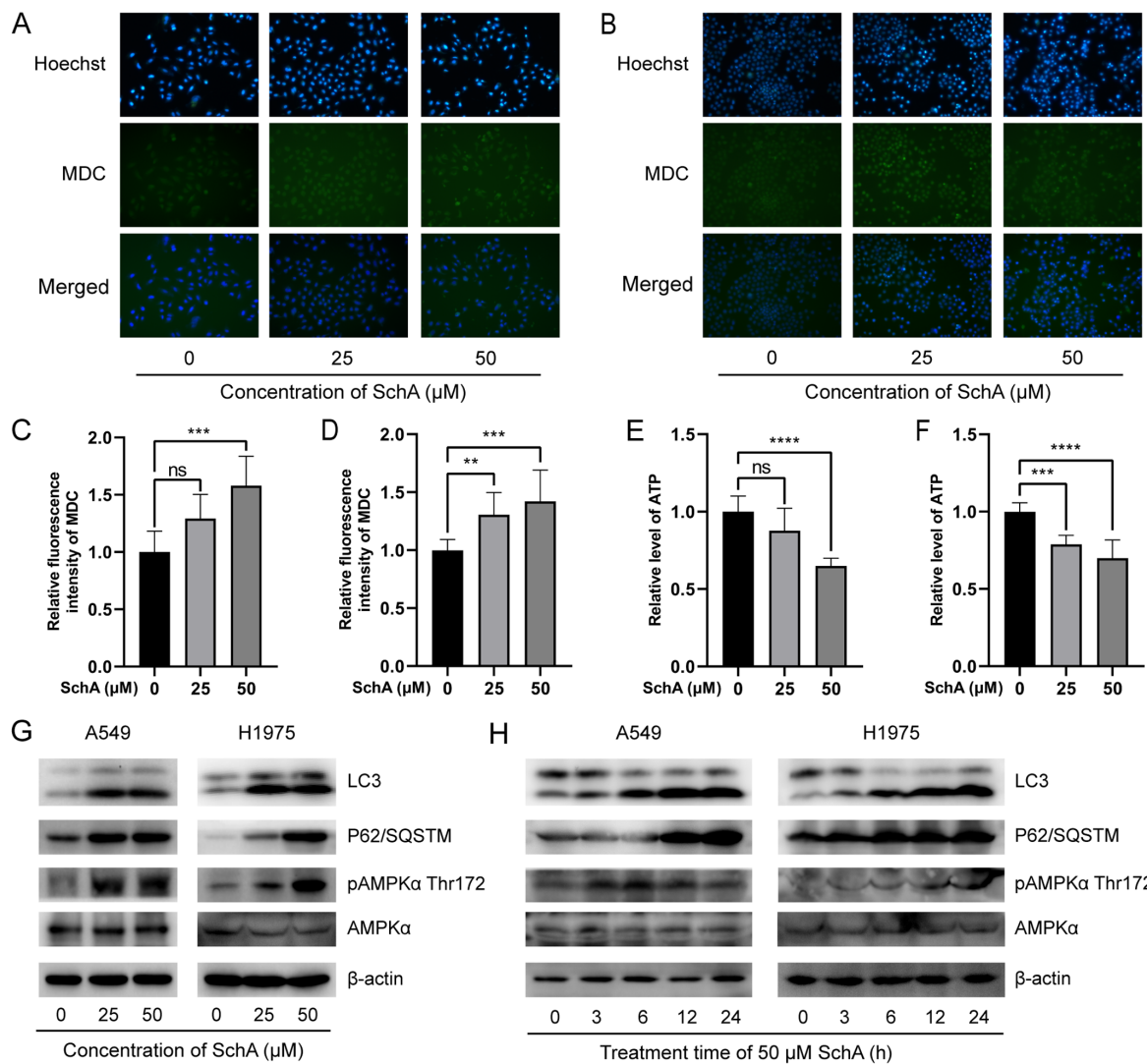


Figure 5. Effects of SchA on autophagy in A549 and H1975 cells. MDC and Hoechst 33342 staining, observed using fluorescence microscopy at x200 magnification showed that SchA caused the blue fluorescence of Hoechst 33342 and the green fluorescence of MDC in the (A) A549 and (B) H1975 cell lines to increase at irregular concentrations. MDC staining measured using a microplate reader showed that SchA significantly increased the fluorescence intensity of MDC in (C) A549 and (D) H1975 cells. SchA reduced intracellular ATP levels in (E) A549 and (F) H1975 cells. (G) As the concentration of SchA increased, the protein expression levels of LC3, p62 and AMPK α -T172 phosphorylation in A549 and H1975 cells were increased. (H) The protein expression levels of LC3, p62/SQSTM1 and AMPK α -T172 phosphorylation in the A549 and H1975 cells were increased following treatment with 50 μ M SchA at different time points. ** P <0.01, *** P <0.001 and **** P <0.0001. MDC, dansylcadaverine; SchA, Schizandrin A; ns, non-significant; p, phosphorylated; AMPK, 5'AMP-activated protein kinase.

also increased after SchA treatment (Fig. 4J). These results suggest that SchA enhanced *Bim* gene transcription in A549 and H1975 cells.

SchA induces autophagy in A549 and H1975 cells. To investigate the effect of SchA on autophagy in A549 and H1975 cells, they were treated with SchA and stained with MDC and Hoechst 33342. Results were then observed by fluorescence microscopy. In the control cells, Hoechst 33342 emitted weak and uniform blue fluorescence whereas MDC emitted uniform yellow/green fluorescence. In the SchA treated cells, Hoechst 33342 showed irregularly concentrated blue fluorescence whilst MDC showed dense green bodies in the cytoplasm (Fig. 5A and B). The blue fluorescence of Hoechst 33342 and the yellow/green fluorescence intensity of MDC were increased as the SchA concentration was increased (Fig. 5A and B).

In addition, a multifunctional microplate reader was used to detect the fluorescence intensity of the MDC-stained cells. Compared with that in the control cells, the green fluorescence intensity in A549 and H1975 cells treated with SchA was significantly increased (Fig. 5C and D).

To verify that SchA activated the autophagy pathway, western blot analysis was used to evaluate the expression levels of the autophagy-related proteins. The results are shown in Fig. 5G and H. As the concentration or the treatment time of SchA increased, the protein expression levels of LC3-II were significantly increased. However, p62 protein expression was increased, suggesting that p62 was not degraded during the autophagic flux. This process was similar to the inhibition of autophagy by chloroquine (CQ) and bafilomycin A1 (BafA1), which inhibited the fusion of autophagosomes and lysosomes (58,59). This observation suggests that whilst SchA did activate autophagy, it hindered

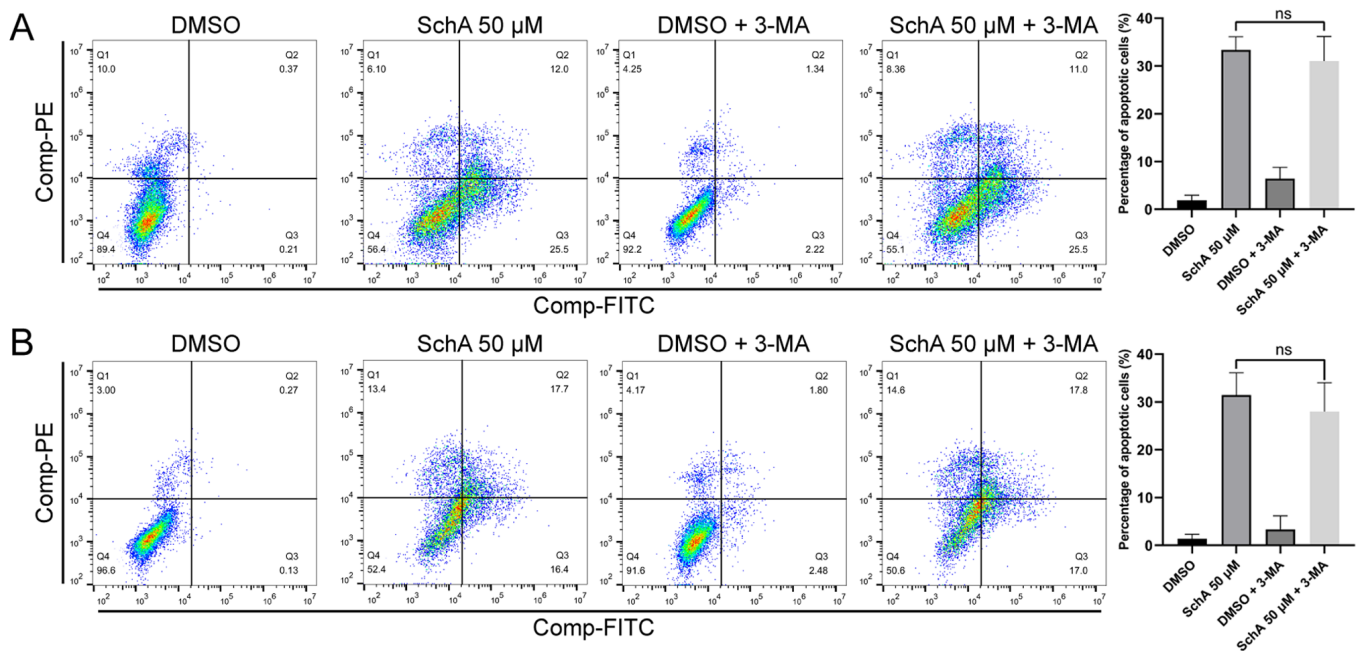


Figure 6. Effects of 3-MA on SchA-induced A549 and H1975 cell apoptosis. Autophagy inhibitor 3-MA has no effects on the apoptosis of (A) A549 and (B) H1975 cells induced by 50 μ M SchA. SchA, Schizandrin A; ns, not significant; 3-MA, 3-methyladenine; ns, non-significant.

the degradation of autophagy substrates, specifically the p62 protein.

SchA induces autophagy in A549 and H1975 cells by reducing ATP levels and activating the AMPK pathway. Insufficient energy and ATP production is an important cause of autophagy in cells (60). In the present study, an ATP detection kit was used to detect the effects of SchA on intracellular ATP levels. As shown in Fig. 5E and F, as the concentration of SchA increased, the intracellular ATP levels were significantly decreased. This suggests that SchA reduced the levels of intracellular ATP.

AMPK is a key intracellular energy sensor (61). Changes in the protein levels of pAMPK α -T172 and AMPK α in A549 and H1975 cells after SchA treatment were measured using western blot analysis. It was found that with increasing the concentration and the treatment time of SchA, markedly increased AMPK α -T172 phosphorylation in A549 and H1975 cells (Fig. 5G and H). This indicated that SchA activated the AMPK signaling pathway in these cells, consistent with the finding that SchA reduced the intracellular ATP levels. This reduction in intracellular ATP levels and activation of the AMPK signaling pathway may be the cause of autophagy induction by SchA.

Effect of inhibiting autophagy on SchA-induced apoptosis. Although SchA-treated A549 and H1975 cells exhibited autophagy activation, this process of autophagy did not result in substrate degradation. Commonly used autophagy inhibitors include 3-methyladenine (3-MA), CQ and BafA1 (62). CQ and BafA1 mainly inhibit the fusion of autophagosomes and lysosomes, whereas 3-MA inhibits autophagosome formation (62). In the present study, the autophagosome formation inhibitor, 3-MA was used to inhibit the early stages of autophagy flux and observe the effects of 3-MA on the cytotoxicity of SchA. After the cells were pre-treated with 3-MA for 4 h, 50 μ M SchA was added to treat the cells for 24 h, before apoptosis

of the cells was measured using flow cytometry. As shown in Fig. 6A and B, the autophagy inhibitor 3-MA did not induce any significant effects on cell apoptosis induced by SchA. This result suggests that SchA-induced autophagy has little impact on apoptosis.

Discussion

Designing or screening drugs based on the biological characteristics of cancer is an effective method of developing novel strategies for treatment (63). In recent years, numerous studies have shown that SchA has anti-tumor effects. Yan and Guo (35) previously reported that 30 μ M SchA could inhibit proliferation, promote apoptosis and inhibit invasion in breast cancer cells. In another study, Xu *et al* (38) reported that 41.4 μ M SchA could inhibit breast cancer cell proliferation and induce cell apoptosis, where the oral administration of SchA (25 mg/kg) could inhibit breast cancer growth in tumor-bearing nude mice. In addition, the weight of the nude mice was not significantly reduced, suggesting that the oral application of SchA was relatively safe (38). Ji and Ma revealed that 50 μ M SchA could inhibit choriocarcinoma cell proliferation, invasion and migration whilst inducing apoptosis (36). In addition, Chen *et al* (37) reported that 68.65 μ M SchA could inhibit the proliferation and colony formation by colorectal cancer cells in addition to inducing apoptosis. Ding *et al* demonstrated that 100 μ M SchA could significantly inhibit the proliferation, invasion and migration of thyroid cancer cells (39). Furthermore, Bi *et al* reported that 30 μ M SchA can inhibit the proliferation and invasion of malignant melanoma cells to induce apoptosis (40). In the present study, SchA was found to inhibit the proliferation of NSCLC cells and induced apoptosis. SchA was cytotoxic to the H1975 cell lines at 39.99 μ M, whilst higher concentrations (101.5 μ M) were required for H1299 cell cytotoxicity. The normal lung epithelial cell line BEAS-2B, was also sensitive

to SchA, which may limit the clinical application of SchA. However, SchA is an important agent for investigation, since it could provide a basic starting point and has the potential for the optimization of more selective and effective, but less toxic derivatives (64).

SchA at low concentrations (10-20 μM) induced G₁/S-phase arrest, whereas high concentrations of SchA ($\geq 30 \mu\text{M}$) caused cell apoptosis. This suggests that SchA caused DNA damage at low concentrations, but the cells could maintain G₁/S-phase arrest to repair the DNA damage. As the concentration of SchA increased and the treatment time was prolonged, the cells gradually lost the ability to maintain the G₁/S-phase arrest and entered the S-phase for DNA replication. DNA replication under stress will lead to fatal DNA damage (65,66), causing a large number of cells to be blocked at the G₂/M cycle checkpoint and undergo cell death.

At low concentrations of SchA, the expression level of the p21 protein increased and the cells were blocked at the G₁/S-phase. As the concentration of SchA increased, the expression level of the p21 protein was decreased, whilst the expression levels of cyclin E2 and CDK2 were increased. This suggests that the increase in p21 may cause SchA-mediated cell G₁/S-phase arrest. However, subsequently the reduction in p21 expression and elevated CDK2 and cyclin E2 expression could cause the cells to overcome G₁/S-phase arrest and enter the S-phase. In colorectal cancer cells, Rehman *et al* (67) found that when the colorectal cancer cells were treated with the chemotherapy drugs irinotecan or FOLFIRI (5-FU, leucovorin and irinotecan), they would enter a slow-dividing, diapause-like, drug-tolerant persister (DTP) state with low energy consumption to resist chemotherapy. Therefore, it was proposed that a precise attack on cancer cells entering the diapause-like DTP state could be an effective method to overcome cancer resistance to chemotherapy (67). In the present study, it was found that G₁/S phase arrest occurred when the cells were damaged by SchA, thereby preventing the cells from entering the S-phase and subsequent apoptosis. G₁/S-phase arrest could also be one of the protection mechanisms of cancer cells (68). Reduction in p21 protein expression and increase in CDK2 and cyclin E2 protein expression could cause DNA-damaged cancer cells to overcome G₁/S phase arrest and enter the S-phase, thereby inducing apoptosis. Therefore, p21, CDK2 and cyclin E2 proteins could potentially be effective targets for overcoming drug resistance in NSCLC cells.

Autophagy is a self-degradation cellular process activated by stress responses, such as starvation, hypoxia or oxidative stress (69). The autophagy mechanism can decompose and recycle intracellular aggregated macromolecular structures or damaged organelles to provide raw materials for the pro-survival metabolic cycle (70). This regulates intracellular homeostasis and assist cells in surviving unfavorable environments (60). Autophagy serves a key role in the development and progression of a variety of tumors, such as lung cancer, breast cancer, stomach cancer, bowel cancer, prostate cancer and pancreatic cancer, and is also one of the main causes of cancer drug resistance (70-75). In the present study, SchA could activate the stress response and induce autophagy in the A549 and H1975 cell lines. However, the autophagy activated by SchA was incomplete, which mainly manifested as the efficient degradation of the autophagy substrate p62.

AMPK is an evolutionarily conserved serine/threonine protein kinase that acts as an energy sensor in cells (76). It serves a crucial role in the activation of catabolism and inactivation of anabolism (61). Under physiological and pathological conditions, AMPK can be phosphorylated by upstream kinases and bind to AMP or ADP instead of ATP, leading to AMPK activation (77). Activated AMPK regulates various metabolic processes, including autophagy (78). AMPK directly promotes autophagy by phosphorylating autophagy-related proteins in the mTOR complex 1, unc-51 like autophagy activating kinase 1 and phosphatidylinositol 3-kinase catalytic subunit type 3 complex, or indirectly promoting autophagy by regulating transcription factors, such as forkhead box O3, transcription factor EB and bromodomain-containing protein 4 (78). In the present study, it was found that SchA reduced the level of intracellular ATP and activated AMPK signaling, which may be one of the mechanisms by which SchA induces autophagy in the NSCLC cell lines.

If autophagy mediates protective effects on cells, then promoting autophagy could inhibit SchA-induced apoptosis and inhibiting autophagy could promote SchA-induced apoptosis. Commonly used inhibitors of autophagy are CQ (79), BafA1 (59), 3-MA (80) and specific and potent autophagy inhibitor-1 (62,81,82). In the present study, the inhibitor 3-MA, which can inhibit the early stage of autophagy (62), was added to inhibit autophagy before the effects of SchA on cell apoptosis was analyzed. It was found that 3-MA did not promote or inhibit SchA-induced cell apoptosis. The present study showed that the incomplete autophagy induced by SchA did not promote cell survival. It was suggested that insufficient autophagy failed to supply recycled materials to sustain pro-survival cellular metabolic processes and maintain homeostasis.

To conclude, the small molecule compound SchA extracted from the medicinal plant Schisandra exerted specific cytotoxic effects on the NSCLC cell lines. When the concentration of SchA is low, it mediated G₁/S-phase cell cycle arrest, whilst at higher concentrations SchA it can cause cell apoptosis. Although, SchA can induce autophagy by activating the AMPK signal, the autophagy process induced by SchA remains incomplete and fails to promote cell survival.

Acknowledgements

Not applicable.

Availability of data and materials

The datasets used and/or analyzed during the current study are available from the corresponding author on reasonable request.

Authors' contributions

LZ and JH designed the study. YW also designed the study and performed the cell viability assays. WL designed the study and performed drug screening and reagent preparation. XW performed the western blotting experiments. HS designed the study and performed the flow cytometry experiments. CH performed the PCR and western blotting experiments. LZ and JH can confirm the authenticity of all the raw data. All authors have read and approved the final version of the manuscript.

Funding

The present study was supported by The Zhejiang Provincial Traditional Chinese Medicine (Integrated Traditional Chinese and Western Medicine) Key Discipline (grant no. 2017-XK-A33), The National Key Research and Development Program (grant no. 2017YFC0113500), The Zhejiang Province Major Science and Technology Special Program Project (grant no. 2020C03058), The Zhejiang Province Lung Tumor Diagnosis and Treatment Technology Research Supported by the Center (grant no. JBZX-202007) and The Zhejiang Medicine and Health General Research Program (grant no. 2019KY069).

Ethics approval and consent to participate

Not applicable.

Patient consent for publication

Not applicable.

Competing interests

The authors declare that they have no competing interests.

References

- International Agency for Research on Cancer (IARC): Latest global cancer data: Cancer burden rises to 19.3 million new cases and 10.0 million cancer deaths in 2020. Questions and Answers (Q&A). <https://www.iarc.who.int/faq/latest-global-cancer-data-2020-qa/>. Accessed January 10, 2021.
- Zheng M: Classification and pathology of lung cancer. *Surg Oncol Clin N Am* 25: 447-468, 2016.
- Duma N, Santana-Davila R and Molina JR: Non-small cell lung cancer: Epidemiology, screening, diagnosis, and treatment. *Mayo Clin Proc* 94: 1623-1640, 2019.
- Siegel RL, Miller KD, Fuchs HE and Jemal A: Cancer Statistics, 2021. *CA Cancer J Clin* 71: 7-33, 2021.
- Jänne PA, Yang JC, Kim DW, Planchard D, Ohe Y, Ramalingam SS, Ahn MJ, Kim SW, Su WC, Horn L, *et al*: AZD9291 in EGFR inhibitor-resistant non-small-cell lung cancer. *N Engl J Med* 372: 1689-1699, 2015.
- Ko B, Paucar D and Halmos B: EGFR T790M: Revealing the secrets of a gatekeeper. *Lung Cancer (Auckl)* 8: 147-159, 2017.
- Shergold AL, Millar R and Nibbs RJ: Understanding and overcoming the resistance of cancer to PD-1/PD-L1 blockade. *Pharmacol Res* 145: 104258, 2019.
- Kobayashi S, Boggon TJ, Dayaram T, Jänne PA, Koehler O, Meyerson M, Johnson BE, Eck MJ, Tenen DG and Halmos B: EGFR mutation and resistance of non-small-cell lung cancer to gefitinib. *N Engl J Med* 352: 786-792, 2005.
- Regales L, Gong Y, Shen R, de Stanchina E, Vivanco I, Goel A, Koutcher JA, Spassova M, Ouerfelli O, Mellinshoff IK, *et al*: Dual targeting of EGFR can overcome a major drug resistance mutation in mouse models of EGFR mutant lung cancer. *J Clin Invest* 119: 3000-3010, 2009.
- Oxnard GR, Yang JC, Yu H, Kim SW, Saka H, Horn L, Goto K, Ohe Y, Mann H, Thress KS, *et al*: TATTON: A multi-arm, phase Ib trial of osimertinib combined with selumetinib, savolitinib, or durvalumab in EGFR-mutant lung cancer. *Ann Oncol* 31: 507-516, 2020.
- Yang JC, Shepherd FA, Kim DW, Lee GW, Lee JS, Chang GC, Lee SS, Wei YF, Lee YG, Laus G, *et al*: Osimertinib plus durvalumab versus osimertinib monotherapy in EGFR T790M-positive NSCLC following previous EGFR TKI therapy: CAURAL Brief Report. *J Thorac Oncol* 14: 933-939, 2019.
- Hanahan D and Weinberg RA: Hallmarks of cancer: The next generation. *Cell* 144: 646-674, 2011.
- Noble RL, Beer CT and Cutts JH: Role of chance observations in chemotherapy: Vinca rosea. *Ann NY Acad Sci* 76: 882-894, 1958.
- Rosenberg B: Platinum coordination complexes in cancer chemotherapy. *Naturwissenschaften* 60: 399-406, 1973.
- Rowinsky EK and Donehower RC: Paclitaxel (taxol). *N Engl J Med* 332: 1004-1014, 1995.
- Zhang H, Bai L, He J, Zhong L, Duan X, Ouyang L, Zhu Y, Wang T, Zhang Y and Shi J: Recent advances in discovery and development of natural products as source for anti-Parkinson's disease lead compounds. *Eur J Med Chem* 141: 257-272, 2017.
- Ying J, Zhang M, Qiu X and Lu Y: The potential of herb medicines in the treatment of esophageal cancer. *Biomed Pharmacother* 103: 381-390, 2018.
- Afanasenko A and Barta K: Pharmaceutically relevant (hetero)cyclic compounds and natural products from lignin-derived monomers: Present and perspectives. *iScience* 24: 102211, 2021.
- Efferth T, Li PC, Konkimalla VS and Kaina B: From traditional Chinese medicine to rational cancer therapy. *Trends Mol Med* 13: 353-361, 2007.
- Szopa A, Ekiert R and Ekiert H: Current knowledge of *Schisandra chinensis* (Turcz.) Baill. (Chinese magnolia vine) as a medicinal plant species: A review on the bioactive components, pharmacological properties, analytical and biotechnological studies. *Phytochem Rev* 16: 195-218, 2017.
- Wang J, Jiang B, Shan Y, Wang X, Lv X, Mohamed J, Li H, Wang C, Chen J and Sun J: Metabolic mapping of *Schisandra chinensis* lignans and their metabolites in rats using a metabolomic approach based on HPLC with quadrupole time-of-flight MS/MS spectrometry. *J Sep Sci* 43: 378-388, 2020.
- Liu M, Zhao S, Wang Z, Wang Y, Liu T, Li S, Wang C, Wang H and Tu P: Identification of metabolites of deoxyschizandrin in rats by UPLC-Q-TOF-MS/MS based on multiple mass defect filter data acquisition and multiple data processing techniques. *J Chromatogr B Analyt Technol Biomed Life Sci* 949-950: 115-126, 2014.
- Liu X, Cong L, Wang C, Li H, Zhang C, Guan X, Liu P, Xie Y, Chen J and Sun J: Pharmacokinetics and distribution of schisandrol A and its major metabolites in rats. *Xenobiotica* 49: 322-331, 2019.
- Jung KY, Lee IS, Oh SR, Kim DS and Lee HK: Lignans with platelet activating factor antagonist activity from *Schisandra chinensis* (Turcz.) Baill. *Phytomedicine* 4: 229-231, 1997.
- Guo M, Lu Y, Yang J, Zhao X and Lu Y: Inhibitory effects of *Schisandra chinensis* extract on acne-related inflammation and UVB-induced photoaging. *Pharm Biol* 54: 2987-2994, 2016.
- Kwon DH, Cha HJ, Choi EO, Leem SH, Kim GY, Moon SK, Chang YC, Yun SJ, Hwang HJ, Kim BW, *et al*: Schisandrin A suppresses lipopolysaccharide-induced inflammation and oxidative stress in RAW 264.7 macrophages by suppressing the NF- κ B, MAPKs and PI3K/Akt pathways and activating Nrf2/HO-1 signaling. *Int J Mol Med* 41: 264-274, 2018.
- Li S, Xie R, Jiang C and Liu M: Schizandrin A alleviates LPS-induced injury in human keratinocyte cell haec through a MicroRNA-127-dependent regulation. *Cell Physiol Biochem* 49: 2229-2239, 2018.
- Chen DF, Zhang SX, Xie L, Xie JX, Chen K, Kashiwada Y, Zhou BN, Wang P, Cosentino LM and Lee KH: Anti-AIDS agents - XXVI. Structure-activity correlations of gomisins-G-related anti-HIV lignans from *Kadsura* interior and of related synthetic analogues. *Bioorg Med Chem* 5: 1715-1723, 1997.
- Ma WH, Lu Y, Huang H, Zhou P and Chen DF: Schisanwilsonins A-G and related anti-HBV lignans from the fruits of *Schisandra wilsoniana*. *Bioorg Med Chem Lett* 19: 4958-4962, 2009.
- Huang M, Jin J, Sun H and Liu GT: Reversal of P-glycoprotein-mediated multidrug resistance of cancer cells by five schizandrins isolated from the Chinese herb *Fructus Schizandrae*. *Cancer Chemother Pharmacol* 62: 1015-1026, 2008.
- Min HY, Park EJ, Hong JY, Kang YJ, Kim SJ, Chung HJ, Woo ER, Hung TM, Youn UJ, Kim YS, *et al*: Antiproliferative effects of dibenzocyclooctadiene lignans isolated from *Schisandra chinensis* in human cancer cells. *Bioorg Med Chem Lett* 18: 523-526, 2008.
- Moon PD, Jeong HJ and Kim HM: Effects of schizandrin on the expression of thymic stromal lymphopoietin in human mast cell line HMC-1. *Life Sci* 91: 384-388, 2012.
- Park JH and Yoon J: Schizandrin inhibits fibrosis and epithelial-mesenchymal transition in transforming growth factor- β 1-stimulated AML12 cells. *Int Immunopharmacol* 25: 276-284, 2015.
- Lin RD, Mao YW, Leu SJ, Huang CY and Lee MH: The immuno-regulatory effects of *Schisandra chinensis* and its constituents on human monocytic leukemia cells. *Molecules* 16: 4836-4849, 2011.

35. Yan H and Guo M: Schizandrin A inhibits cellular phenotypes of breast cancer cells by repressing miR-155. *IUBMB Life* 72: 1640-1648, 2020.
36. Ji L and Ma L: MEG3 is restored by schisandrin A and represses tumor growth in choriocarcinoma cells. *J Biochem Mol Toxicol* 34: e22455, 2020.
37. Chen BC, Tu SL, Zheng BA, Dong QJ, Wan ZA and Dai QQ: Schizandrin A exhibits potent anticancer activity in colorectal cancer cells by inhibiting heat shock factor 1. *Biosci Rep* 40: 40, 2020.
38. Xu X, Rajamanicham V, Xu S, Xu S, Liu Z, Yan T, Liang G, Guo G, Zhou H, Wang Y, *et al*: Schisandrin A inhibits triple negative breast cancer cells by regulating Wnt/ER stress signaling pathway. *Biomed Pharmacother* 115: 108922, 2019.
39. Ding Q, Li X, Sun Y and Zhang X: Schizandrin A inhibits proliferation, migration and invasion of thyroid cancer cell line TPC-1 by down regulation of microRNA-429. *Cancer Biomark* 24: 497-508, 2019.
40. Bi Y, Fu Y, Wang S, Chen X and Cai X: Schizandrin A exerts anti-tumor effects on A375 cells by down-regulating H19. *Braz J Med Biol Res* 52: e8385, 2019.
41. Lee K, Ahn JH, Lee KT, Jang DS and Choi JH: Deoxyschizandrin, isolated from Schisandra berries, induces cell cycle arrest in ovarian cancer cells and inhibits the protumoural activation of tumour-associated macrophages. *Nutrients* 10: 10, 2018.
42. Kim SJ, Min HY, Lee EJ, Kim YS, Bae K, Kang SS and Lee SK: Growth inhibition and cell cycle arrest in the G0/G1 by schizandrin, a dibenzocyclooctadiene lignan isolated from *Schisandra chinensis*, on T47D human breast cancer cells. *Phytother Res* 24: 193-197, 2010.
43. Xian H, Feng W and Zhang J: Schizandrin A enhances the efficacy of gefitinib by suppressing IKK β /NF- κ B signaling in non-small cell lung cancer. *Eur J Pharmacol* 855: 10-19, 2019.
44. Kong D, Zhang D, Chu X and Wang J: Schizandrin A enhances chemosensitivity of colon carcinoma cells to 5-fluorouracil through up-regulation of miR-195. *Biomed Pharmacother* 99: 176-183, 2018.
45. Zhang ZL, Jiang QC and Wang SR: Schisandrin A reverses doxorubicin-resistant human breast cancer cell line by the inhibition of P65 and Stat3 phosphorylation. *Breast Cancer* 25: 233-242, 2018.
46. Su X, Gao C, Shi F, Feng X, Liu L, Qu D and Wang C: A micro-emulsion co-loaded with Schizandrin A-docetaxel enhances esophageal carcinoma treatment through overcoming multidrug resistance. *Drug Deliv* 24: 10-19, 2017.
47. Livak KJ and Schmittgen TD: Analysis of relative gene expression data using real-time quantitative PCR and the 2⁻(Delta Delta C(T)) method. *Methods* 25: 402-408, 2001.
48. Ng KP, Hillmer AM, Chuah CT, Juan WC, Ko TK, Teo AS, Ariyaratne PN, Takahashi N, Sawada K, Fei Y, *et al*: A common BIM deletion polymorphism mediates intrinsic resistance and inferior responses to tyrosine kinase inhibitors in cancer. *Nat Med* 18: 521-528, 2012.
49. Opletal L, Sovová H and Bártlová M: Dibenzo[a,c]cyclooctadiene lignans of the genus Schisandra: Importance, isolation and determination. *J Chromatogr B Analyt Technol Biomed Life Sci* 812: 357-371, 2004.
50. Zheng S, Aves SJ, Laraia L, Galloway WR, Pike KG, Wu W and Spring DR: A concise total synthesis of deoxyschizandrin and exploration of its antiproliferative effects and those of structurally related derivatives. *Chemistry* 18: 3193-3198, 2012.
51. Newbold A, Martin BP, Cullinane C and Bots M: Detection of apoptotic cells using propidium iodide staining. *Cold Spring Harb Protoc* 2014: 1202-1206, 2014.
52. Pan X, Zhao J, Zhang WN, Li HY, Mu R, Zhou T, Zhang HY, Gong WL, Yu M, Man JH, *et al*: Induction of SOX4 by DNA damage is critical for p53 stabilization and function. *Proc Natl Acad Sci USA* 106: 3788-3793, 2009.
53. Santos JH, Hunakova L, Chen Y, Bortner C and Van Houten B: Cell sorting experiments link persistent mitochondrial DNA damage with loss of mitochondrial membrane potential and apoptotic cell death. *J Biol Chem* 278: 1728-1734, 2003.
54. Yang Y, Karakhanova S, Hartwig W, D'Haese JG, Philippov PP, Werner J and Bazhin AV: Mitochondria and mitochondrial ROS in cancer: Novel targets for anticancer therapy. *J Cell Physiol* 231: 2570-2581, 2016.
55. Chen M, Guerrero AD, Huang L, Shabier Z, Pan M, Tan TH and Wang J: Caspase-9-induced mitochondrial disruption through cleavage of anti-apoptotic BCL-2 family members. *J Biol Chem* 282: 33888-33895, 2007.
56. Willis SN and Adams JM: Life in the balance: How BH3-only proteins induce apoptosis. *Curr Opin Cell Biol* 17: 617-625, 2005.
57. Bouillet P, Zhang LC, Huang DC, *et al*: Gene structure alternative splicing, and chromosomal localization of pro-apoptotic Bcl-2 relative Bim. *Mamm Genome* 12: 163-168, 2001.
58. Mauthe M, Orhon I, Rocchi C, Zhou X, Luhr M, Hijiikema KJ, Coppes RP, Engedal N, Mari M and Reggiori F: Chloroquine inhibits autophagic flux by decreasing autophagosome-lysosome fusion. *Autophagy* 14: 1435-1455, 2018.
59. Mauvezin C and Neufeld TP: Bafilomycin A1 disrupts autophagic flux by inhibiting both V-ATPase-dependent acidification and Ca-P60A/SERCA-dependent autophagosome-lysosome fusion. *Autophagy* 11: 1437-1438, 2015.
60. Kim KH and Lee MS: Autophagy - a key player in cellular and body metabolism. *Nat Rev Endocrinol* 10: 322-337, 2014.
61. Ha J, Guan KL and Kim J: AMPK and autophagy in glucose/glycogen metabolism. *Mol Aspects Med* 46: 46-62, 2015.
62. Pasquier B: Autophagy inhibitors. *Cell Mol Life Sci* 73: 985-1001, 2016.
63. Seebacher NA, Stacy AE, Porter GM and Merlot AM: Clinical development of targeted and immune based anti-cancer therapies. *J Exp Clin Cancer Res* 38: 156, 2019.
64. Keglevich P, Hazai L, Kalas G and Szántay C: Modifications on the basic skeletons of vinblastine and vincristine. *Molecules* 17: 5893-5914, 2012.
65. Gaillard H, García-Muse T and Aguilera A: Replication stress and cancer. *Nat Rev Cancer* 15: 276-289, 2015.
66. Cortez D: Replication-coupled DNA repair. *Mol Cell* 74: 866-876, 2019.
67. Rehman SK, Haynes J, Collignon E, Brown KR, Wang Y, Nixon AM, Bruce JP, Wintersinger JA, Singh Mer A, Lo EB, *et al*: Colorectal cancer cells enter a Diapause-like DTP state to survive chemotherapy. *Cell* 184: 226-242.e21, 2021.
68. Recasens A and Munoz L: Targeting cancer cell dormancy. *Trends Pharmacol Sci* 40: 128-141, 2019.
69. Glick D, Barth S and Macleod KF: Autophagy: Cellular and molecular mechanisms. *J Pathol* 221: 3-12, 2010.
70. Li YJ, Lei YH, Yao N, Wang CR, Hu N, Ye WC, Zhang DM and Chen ZS: Autophagy and multidrug resistance in cancer. *Chin J Cancer* 36: 52, 2017.
71. Farrow JM, Yang JC and Evans CP: Autophagy as a modulator and target in prostate cancer. *Nat Rev Urol* 11: 508-516, 2014.
72. Liu G, Pei F, Yang F, Li L, Amin AD, Liu S, Buchan JR and Cho WC: Role of autophagy and apoptosis in non-small-cell lung cancer. *Int J Mol Sci* 18: 18, 2017.
73. Piffoux M, Eriau E and Cassier PA: Autophagy as a therapeutic target in pancreatic cancer. *Br J Cancer* 124: 333-344, 2021.
74. Zarzynska JM: The importance of autophagy regulation in breast cancer development and treatment. *BioMed Res Int* 2014: 710345, 2014.
75. Zhou H, Yuan M, Yu Q, Zhou X, Min W and Gao D: Autophagy regulation and its role in gastric cancer and colorectal cancer. *Cancer Biomark* 17: 1-10, 2016.
76. Hardie DG, Ross FA and Hawley SA: AMPK: A nutrient and energy sensor that maintains energy homeostasis. *Nat Rev Mol Cell Biol* 13: 251-262, 2012.
77. Lin SC and Hardie DG: AMPK: Sensing Glucose as well as Cellular Energy Status. *Cell Metab* 27: 299-313, 2018.
78. Li Y and Chen Y: AMPK and autophagy. *Adv Exp Med Biol* 1206: 85-108, 2019.
79. Kimura T, Takabatake Y, Takahashi A and Isaka Y: Chloroquine in cancer therapy: A double-edged sword of autophagy. *Cancer Res* 73: 3-7, 2013.
80. Wu YT, Tan HL, Shui G, Bauvy C, Huang Q, Wenk MR, Ong CN, Codogno P and Shen HM: Dual role of 3-methyladenine in modulation of autophagy via different temporal patterns of inhibition on class I and III phosphoinositide 3-kinase. *J Biol Chem* 285: 10850-10861, 2010.
81. Levy JMM, Towers CG and Thorburn A: Targeting autophagy in cancer. *Nat Rev Cancer* 17: 528-542, 2017.
82. Pesce E, Sondo E, Ferrera L, Tomati V, Caci E, Scudieri P, Musante I, Renda M, Baatallah N, Servel N, *et al*: The autophagy inhibitor Spautin-1 antagonizes rescue of mutant CFTR through an autophagy-independent and USP13-mediated mechanism. *Front Pharmacol* 9: 1464, 2018.

